Methods

1. Modelling Planetary Density Functions coming from Interference Processes and Exponential Distortion of Planetary Positions

To model the interference processes, access density functions associated with planetary domains, and perform the exponential distortion of planetary positions, I used **SciDavis**, a scientific data analysis and visualization software. This software is well-suited for interpolating experimental data, such as planetary positions, and provides tools for defining and applying the necessary functions to simulate diffraction interference processes with exponential effects. SciDavis enables the generation of distorted interference patterns that accurately reproduce planetary positions and their associated dynamical functions.

2. Mathematical Interpretation

In order to obtain the subsequent features arising from the interaction interference process occurring on a possible transmission grating, I performed a simple analysis of the positions of the planets, starting with the telluric ones reported in table M1.

m^{th} (interference order)	***Planet***	***Heliocentric Average Distance(A.U.)***
-2	Venus	-0.72
0	Sun	0
+1	Mercury	0.39
+2	Earth	1
+3	Mars	1.52

Table M1: The experimental data collected and associated with the interference orders, determined empirically based on planetary positions and structural similarities, particularly between Venus and Earth.

I determined their possible interference order based on common characteristics and interpolated the data. Using SciDavis, I obtained the following graphs:

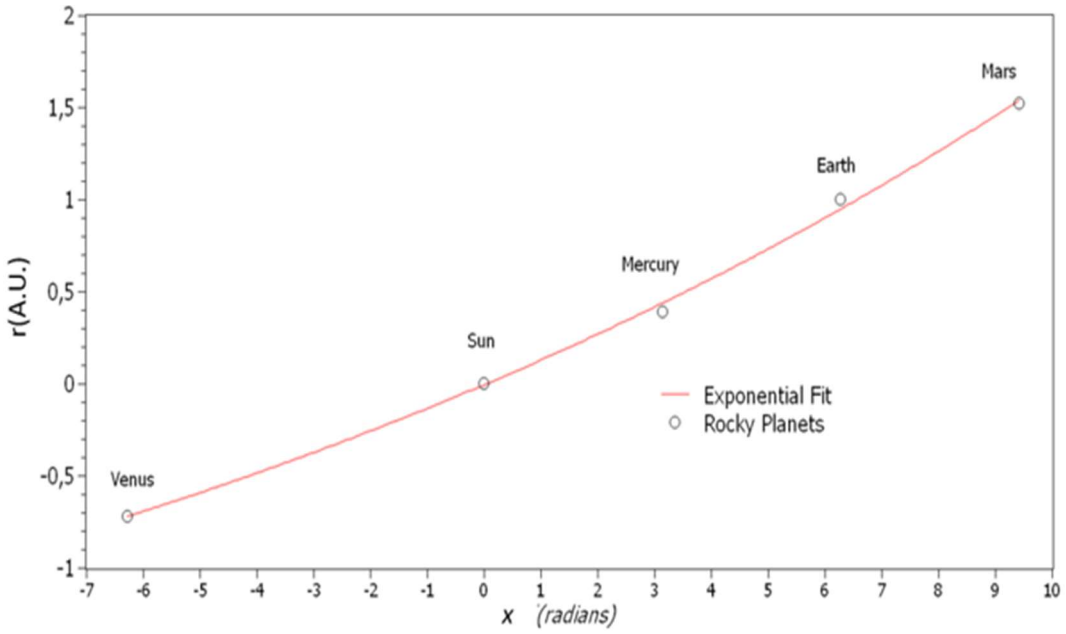

Figure M1 The average distances of the terrestrial planets from the Sun are represented by white dots. The best fit for these planetary distances, as a function of their mmmth interference order (expressed in radians), follows a first-order exponential growth of the form, $r_{max} = A(e^{m\theta} - 1)$. The red curve represents the results of this fit, where the parameter *A* corresponds to the origin of the diffraction-interference pattern, and θ denotes the constructive interference angle at which the maxima of the diffraction-interference pattern *(m)* occur.

Through this procedure, I aimed to determine the unknown origin of incoming cosmic winds scattering. Knowing that, from the slight exponential distortion in the Taylor limit of stopping at the first order, the problem could be reduced to the classical Fraunhofer conditions for an interference process, which can be expressed as $r_{max} = \pm m L_0 \theta_{diff}$.

The exponential relation interpolating the planetary positions offered the equation:

$$r_{max}\ (A.U.) = 2.9\left(e^{\frac{m\pi}{21}} - 1\right) \qquad (1)$$

That through Taylor expansion offered the $\theta_{diff} = \frac{\pi}{21} = 8° \pm 0.4°$ *and* $L_0 = 2.9 \pm 0.05$ *(A.U)* identifying a region of scattering for incoming radiation. Notably, this region aligns well with the Main Asteroid Belt (MAB), precisely where one of the main Kirkwood Gaps is located.
Using the modified Fraunhofer equation derived in Equation (1), the resulting interference pattern is shown in **Figure 1** of the main text relative to the telluric planets.
Starting from this basic observation, I reinterpreted the Kirkwood Gaps as scattering regions, where the observed lack of asteroids (as shown in Figure M2) corresponds to well-focused beams of incoming micrometeoritic material. This influx has been modelled using Gaussian flux distributions, concentrating in three main regions.

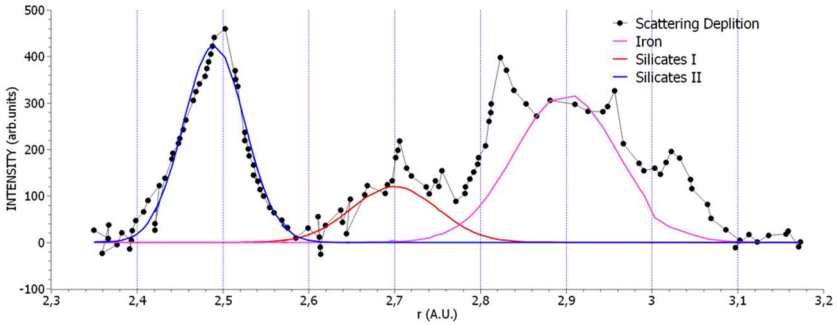

Figure M2: Interpretation of Kirkwood depletion areas by a Gaussian Fit. Three main peaks can be observed. Xc1= 2.9(A.U.) (purple Curve), Xc2= 2.7 (A.U.) Red Curve and Xc3= 2.5(A.U.) Blue Curve. The proposed interpretation of the void regions, considered the features related to iron micrometeorites scattering (2.9.A.U.) and Silicates I and II scattering (2.7 and 2.5A.U.) respectively.

The observed distribution of asteroid depleted densities, gave me the opportunity to make a possible Fit via three Gaussians functions, which vary in position, intensity and FWHM. The results obtained are reported in Table 3.1.

Peak Position Xc (A.U.)	**Area (arb.units) A**	**FWHM (A.U.) W**
2.9±0.08	48±3	0.12±0.02
2.7±0.08	15±2	0.10±0.01
2.46±0.05	38±2	0.075±0.002

Table M2: Reproted results of the Best Fit of Kirkwood's Gaps consdering the three Gsussian functions shown in Figure M2.

In this innovative interpretation, Kirkwood Gaps are the result of the scattering processes of incoming cosmic winds over the orbiting asteroids of the MAB, each contributing chemically to the final planetary configuration. Therefore, an analytical process was conducted to determine the scattering events that occurred and to identify the planetary accretion processes involved, using the diffraction-interference procedure detailed in Supplementary Notes 1.

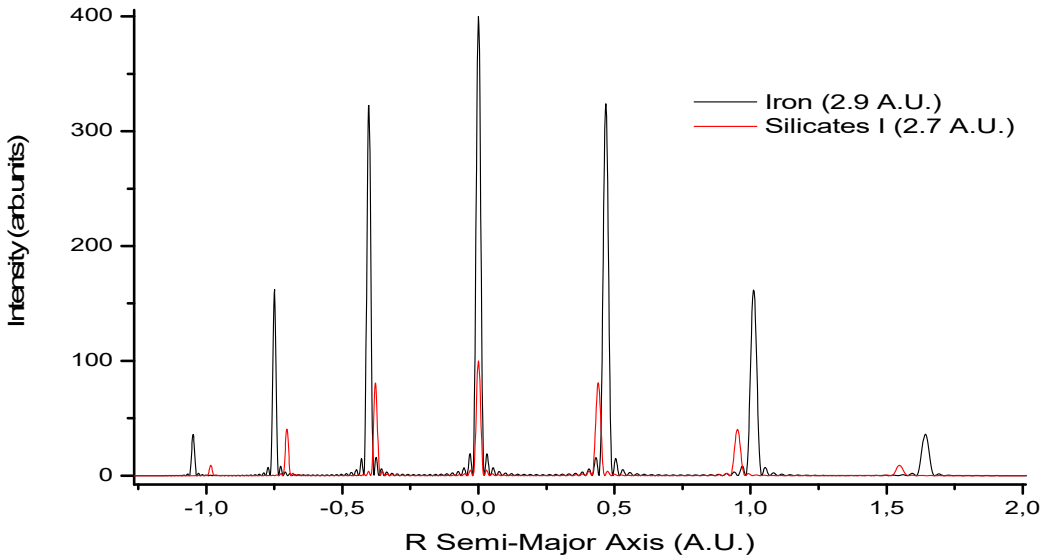

Figure M3: The graph illustrates the diffraction-interference asymmetric progressions due to scattering at 2.9 and 2.7 A.U. within the Main Asteroid Belt (MAB). The two exponentially distorted representations of simple interference processes determine the various components of the telluric planets, with their intensity modulated by the areas found for the respective Kirkwood gaps, as reported in Table 2. In the graph, the Iron/Nickel component (black continuous line) represents the M-type scattered chondritic star winds, while the S-type component, associated with silicates, is also indicated.

From this initial analysis, as shown in Figure M3, it became evident that if planetary formation were driven by the same scattering conditions for each Kirkwood gap, more planets should have been observed, since the external regions of the graph (R<-0.6 AU and R>+1 AU) exhibited very little overlap between the interference features. However, the increased dimensions of Earth and Venus, compared to the rest of the telluric planets, led me to suggest that the scattering events at 2.7 AU and 2.5 AU correspond to the accretion of only the second-order features of the primary 2.9 AU interference process.

If the exponential distortion occurred differently throughout the scattering processes at the MAB, differential accretion could be established. Hence the second-order of interference effect of the 2.9 A.U. could gain incremented accretion compared to the other features of the same scattering process.

Through this hypothesis I obtained the following equations:

$$r(\theta) = 2.5\left(e^{\frac{m\pi}{9.2}} - 1\right) \qquad (2)$$

And

$$r(\theta) = 2.7\left(e^{\frac{m\pi}{10}} - 1\right) \qquad (3)$$

Which would yield the following diffraction interference features, leading to the exclusive accretion of Earth and Venus.

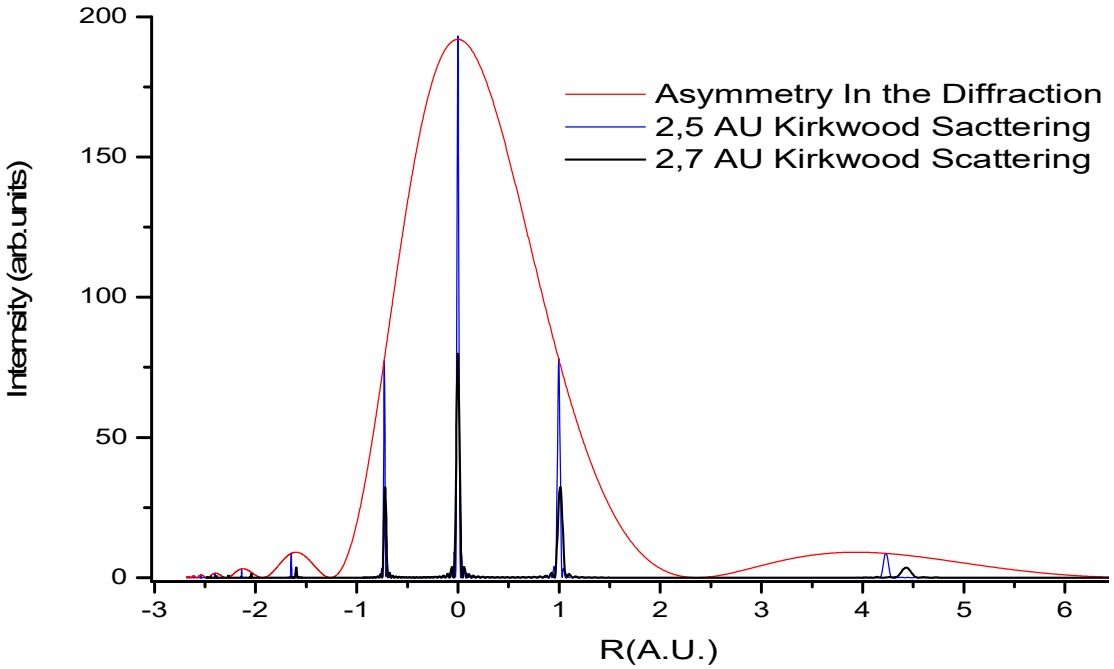

Figure M4: The Asymmetric Diffraction/Interfecene progressions considering the $\boldsymbol{r(\theta) = -2.5 + 2.5\, e^{\left(\frac{m\pi}{9.2}\right)}}$ and $\boldsymbol{r(\theta) = -2.7 + 2.7\, e^{\left(\frac{m\pi}{10}\right)}}$ and suggesting a Diffraction modulation (red continuos line) and 2nd order interferecne suppression justifying accretion for Earth and Venus, and more minor fetures which can be associated to satellite fomations epecially in the region where Jupiter is Formed (4 < R < 5 AU).

This interpretation separates the scattering processes that occurred at the Main Asteroid Belt (MAB) into two groups, leading to the formation of larger telluric planets due to an excess of scattered material preferentially directed toward Earth and Venus, specifically within the inner Kirkwood Gaps region (2.5–2.7 AU). These processes coherently overlapped with second-order interference, contributing to the increased dimensions of Earth and Venus, as shown in **Figure 3** of the main text. Here, Figure M5 specifically highlights the region associated with Earth and the 0th order being the Sun in its telluric contribution to its overall density function.

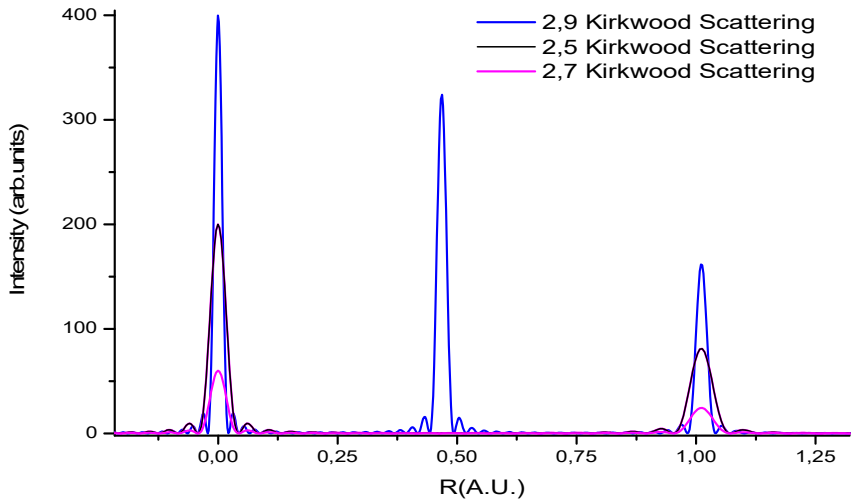

Figure M5: The overlap between the 2.9 (AU) Black Curve interference driven scattering and the 2.7(AU) component contributing to the 2nd order of interference accretion. The two interference processes have different intensities since they were scaled according to the major multiplicative factors *A* obtained by the Gaussian fit proposed in **Figure M2** and reported in **Table M2**. Additionally, the Mercury density function around 0.4 AU is reported, showing that its only significant contribution originates from the 2.9 AU scattering process

The relation (2) and (3) found have led to $\mathbf{L_0}$=2.7 AU and $\boldsymbol{\theta_{diff}} = \frac{\pi}{9.2} = 19° \pm 0.5°$; $\boldsymbol{L_0}$=2.5AU, $\boldsymbol{\theta_{diff}} = \frac{\pi}{10} = 18° \pm 0.5°$ suggesting that the effect of the different chemical compositions of the scattering incoming cosmic winds have given different interference conditions producing differential planetary accretion. The same level of detail regarding depletion, as observed for the Main Asteroid Belt (MAB) by Kirkwood, is not available for the Kuiper Belt, which is responsible for the formation of Gas and Ice giants. However, as shown in **Supplementary Note 3**, it is evident that these planets did not undergo a differential accretion model. This supports the idea that the incoming flux responsible for the formation of the Gas Giants was a single, unified event, in contrast to the inner telluric planets, which experienced a multiple accretion process.

3. Mathematical Models and Simulations

Particular attention in the present work has been given to the region where the Earth has been formed so to give the most adherent representation of the system of our Blue Planet.

- **Model Overview:** The modelling of Earth's density function, $\Phi(\rho)_{Earth}$, began with the interpretation of data from the previous section, which explicitly determines that the scattering process at the Kirkwood Gaps produced different yields, influencing the overall formation of the planet. Notably, the scattering process could not overlap in the same way as it would in a photonic representation of the interference process, since the scattered particles in this case possess mass, unlike photons.
- **The Technique:** The specific density functions calculated, properly scaled according to the intensity established through the relative depletion of the Kirkwood Gaps (as shown in Table 2), have been adjusted to correspond to the observed density of Earth via A multiple regression Fit obtained through SciDavis program. The experimentally observed density instead is reported in the main text in ***Figure 3*** as a black step function, whose values are consistent with geological data and are categorized into distinct layers: inner core, outer core, inner mantle, outer mantle, crust, and atmosphere.

4. Data Analysis

Each density distribution function associated to the interference profile $\Psi^2(r)_{p\pm i}$ can be approximated by a Gaussian function of the form:

$$Y(i) = Ai \cdot \frac{\sqrt{2/\pi}}{w1} \cdot e^{-2\frac{(x-x_0)^2}{(wi)^2}} \qquad (4)$$

According to the constraints enumarted in the technique section, the best fit to the experimental observations has been achieved using the following relation:

$$\Phi(\rho_{Earth}) = \boldsymbol{A}(Y1) + \boldsymbol{B}(Y2) + \boldsymbol{C}(Y3) \qquad (5)$$

Since the densest configuration corresponds to Earth's core, which originates from the 2.9 AU Kirkwood gap scattering (A)—a feature observed in all inner telluric planets—the other components, B and C, represent the mantle's inner and outer layers. These components collectively determine the final density distribution obtained through multiple regression analysis:

$$\Phi(\rho_{Earth}) = \underbrace{\frac{5x10^5}{3500}\cdot\sqrt{\frac{2}{\pi}}e^{-2\frac{(x-0)^2}{(3500)^2}}}_{\boldsymbol{A(Y1)}} + \underbrace{\frac{2.27x10^5}{3000}\cdot\left(\sqrt{\frac{2}{\pi}}e^{-2\frac{(x+4265)^2}{(3000)^2}} + \sqrt{\frac{2}{\pi}}e^{-2\frac{(x-4265)^2}{(3000)^2}}\right)}_{\boldsymbol{B(Y2)}}$$

$$+ \underbrace{\frac{1.15x10^5}{2556}\cdot\left(\sqrt{\frac{2}{\pi}}e^{-2\frac{(x+2265)^2}{(2556)^2}} + \sqrt{\frac{2}{\pi}}e^{-2\frac{(x-226\ )^2}{(2556)^2}}\right)}_{\boldsymbol{C(Y3)}} \qquad (6)$$

Leading to **Figure 3** in the main text.

Approximations: The approximation consists of considering the entire density function as symmetrical, in accordance with the nature of the Gaussian functions used to determine Earth's density function. Moreover, a portion of the scattering from the 2.5–2.7 AU region may have influenced part of the core density. However, within the limits of this approximation—which accounts for only three main scattering events out of the nine overall structures reported in Supplementary Figure 6—the overall contribution remains well within the error margin of 10-15% relative to the experimental density function.

In order to extract fundamental parameters such as atmospheric density ρ_{Air} and the gravitational acceleration of the planet **g**, I determined that this initial approximation of the real density function, represented by $\Phi(\rho)$, could undergo further simplification into an interference-like mathematical function such ads the $\cos^2$ () function shown below by the red curve.

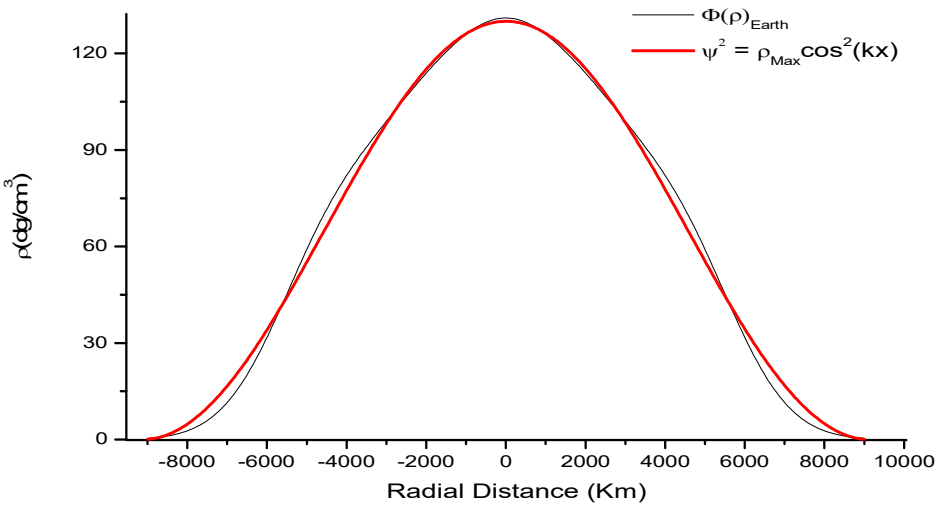

Figure M6: The calculated density function $\Phi(\rho)$ is reported as the black continuous line. A best-fit analysis using the $\cos^2$ function was performed to extract fundamental parameters for the planet is shown (—).

$$\Phi(\rho) \approx \rho_{max}\cos^2(kx) \quad (7)$$

The resulting analysis provided $\rho_{max} = 120 dg/cm^3$ and $k = 1.9x10^{-4} (rad/Km)$.

And considering Poisson equation of relating the force to the gradient of the potential, by performing the first derivative of equation (7) we obtain:

$$\Phi'(\rho)_{Earth} \approx k\rho_{Max}\sin[2(k\Delta x)] \qquad (8)$$

From basic calculations, we obtain:

$$k\rho_{Max} \approx 2\rho_{Air}$$

By executing a series expansion of the sine function, the acceleration **g** acting in the region *Δx at the surface* (the diameter of the planet) where the planet is forming can be obtined:

$$|\boldsymbol{f}| = \Phi'(\Delta x) \approx -4k\Delta x\, \rho_{Air} \approx \boldsymbol{g}\rho_{Air} \qquad (9)$$

Relation (9) indicates that the system being formed through its $\Phi(\rho)$ contains the necessary elements to observe a specific atmosphere, subject to the required gravitational acceleration γ_p, definite for each planetary formation:

According to this observation, in the ideal case where the spatial region Δx in which the planet is forming is completely void, an ideal mass of density *(i)*, influent to the final acceleration γ_p, shapes the term $k\rho_{Max}$ in (8) to the form $2k(i)\,\gamma_p$ leading to a most general case:

$$\Phi'(\rho) \approx 2k(i)\,\gamma_p\,[2(k\Delta x)] \qquad (10)$$

The factor of 2 in relation (10) results from a successful ideal inelastic collision between two masses subjected to the same acceleration $\boldsymbol{\gamma_p}$, acting within the spatial region **Δx**, which leads to the diameter of the solid planet. This process is determined by the two density function distributions of the opposing scattering interference events, as shown in **Supplementary Note 2**, and schematically represented in **Figure M7**.

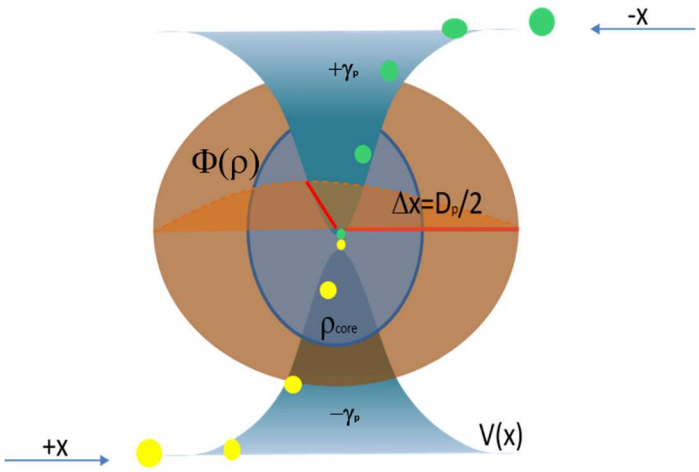

Figure M7: The incoming ideal masses of density *(i)*, represented in yellow and green, approach from opposite directions (±x), as established in **Supplementary Note 2**. While moving through space unaffected, they experience acceleration $\boldsymbol{\gamma_p}$ upon entering the blue region, where the interference process acts on them. This interaction results in the final planetary density distribution Φ(ρ)**.**

and assuming *(i)* as a symbolic unit of density coming from outer space, and recalling that the $k\Delta x=\pi$ a general semi-empirical relation for the gravitational constant γ_p can be written:

$$\gamma_p \approx \frac{\Phi'(\rho)}{4\pi k(i)} \qquad (11)$$

and specifically, since the observed gravitational acceleration at the surface has paramount importance to shape planetary atmospheric conditions:

$$g_p \approx \frac{\Phi'(\rho_{surf})}{4\pi k(i)} \qquad (12)$$

Where $\Phi'(\rho_{surf})$ can be confidently approximated to the tangent to the density function at the surface of the planet.

In the case of Earth by inserting the calualetd values of $\Phi'(\rho_{Surf})_{Earth}$= *0.024±0.005 dg/cm^3(m/s^2)(rad/Km) and k=1.9x10^{-4}rad/Km then the calculated* $\boldsymbol{g_{Earth}}$**=10.05±0.3m/s^2** per unit of density, *(i) dg/cm^3* , that is in good agreement with the known value of **g=9.8m/s^2**.